Role of Skyrme forces in cluster radioactivity of parent nuclei with even (A, Z)

Rajni [1,2,*] Gudveen Sawhney [3] and Manoj K. Sharma [2]

[1]*Department of Physics, Sardar Vallabhbhai National Institute of Technology, Surat 395007, Gujarat, India*
[2]*School of Physics and Materials Science, Thapar Institute of Engineering and Technology, Patiala 147004, Punjab, India*
[3]*Department of Physics, University Institute of Sciences, Chandigarh University, Gharuan, Mohali 140413, Punjab, India*

(Received 20 July 2022; accepted 20 September 2022; published 19 October 2022)

We investigate the role of different Skyrme forces (SIII, SkI4, and SAMi) in the ground state decay of various radioactive parent nuclei such as Ra, Th, U, and Pu. The daughters of these nuclei are either doubly magic ^{208}Pb or a nearby isotope of Pb. Using spherical choice of cluster and daughter, calculations are performed within the framework of the preformed cluster model (PCM), where the preformation probability P_0 and penetration probability P of decaying fragments are used to obtain the half-lives of cluster emission. The considered forces modify the barrier characteristics and consequently the penetration path, as the scattering potential at the first turning point of the barrier is lowest with the SkI4 force (lowest penetrability) and highest with the SIII force (highest penetrability). However, the preformation probability of decaying clusters is highest for the SkI4 force followed by SAMi and SIII Skyrme forces. To look for the possible role of the spin-orbit effect on the cluster radioactivity, the half-lives of emitted clusters are calculated with and without the inclusion of spin-orbit potential V_J. In addition, the α-decay half live are also calculated to extract an inclusive picture of the dynamics involved.

DOI: 10.1103/PhysRevC.106.044605

I. INTRODUCTION

The phenomenon of cluster radioactivity (CR) has intrigued researchers working in this area. Multiple studies were conducted by diverse experimental groups at Berkeley, Dubna, Orsay, and Milano to investigate this extremely rare decay mechanism of heavy nuclei [1–3]. Sandulescu, Poenaru, and Greiner [4] initially predicted CR in 1980, and Rose and Jones [5] confirmed it in 1984 for ^{14}C radioactivity from the ^{223}Ra nucleus. Since then, the emissions of ^{14}C, ^{20}O, ^{23}F, ^{22,24,26}Ne, ^{28,30}Mg, and ^{32,34}Si clusters have been observed experimentally in the mass region where parent nuclei with charge $Z = 87$–96 are found. All these measured decays result in daughter nuclei that are doubly magic or almost doubly magic (i.e., ^{208}Pb or closely neighboring nuclei). This suggests that the shell effect plays a crucial role in the cluster emission for heavy nuclei. Interestingly, Poenaru *et al.* [6] projected emission of relatively heavier clusters ($Z_c > 28$), named heavy cluster radioactivity, from parents with $Z > 110$ and daughters around ^{208}Pb, implying the possibility of another decay mechanism from superheavy nuclei.

The half-lives of various cluster decay modes have been investigated using various models such as the analytical superasymmetric fission model (ASAFM) [6], the unified description (UD) formula [7], the universal curve for α and cluster radioactive decay [8], the universal decay law (UDL) [9], the Horoi formula [10], and the cubic plus Yukawa plus exponential model (CYEM) [11,12]. In addition to these, the Bardeen-Cooper-Schrieffer (BCS) approach has also been used to study cluster decay with reasonable success [13]. In general, two types of models, cluster-like models [14–18] and fission-like models [6,19,20], are used to describe the cluster radioactivity. In the cluster-like hypothesis, the cluster is assumed to form in the parent nucleus before breaking through the potential barrier. However within a fission model, the formation probability of a cluster is calculated as a penetration of the internal part of the barrier.

In our earlier work, some of us and co-authors investigated the role of deformations for the exotic decays of radioactive nuclei from the trans-Pb region using the preformed cluster model (PCM) [14–18]. The deformations up to quadrupole, as well as the selection of "optimal" orientations, were found [14,15] to be sufficient to address the experimental data on half-lives using the model's only parameter, the neck-length parameter ΔR. With the use of "compact" orientations, the role of higher-multipole deformations was later accounted for in the decay of ^{14}C clusters [16]. Later on, various types of nuclear proximity potentials were employed [21] for comprehensive knowledge of cluster dynamics involving ^{208}Pb and non-^{208}Pb as a daughter nucleus. In the present work, we take up this study on the basis of the preformed cluster model (PCM) to analyze the influence of Skyrme forces on the behavior of possible fragmentation of ^{222}Ra, ^{224}Ra, ^{226}Ra, ^{226}Th, ^{228}Th, ^{230}Th, ^{230}U, ^{232}U, ^{234}U, ^{236}Pu, and ^{238}Pu parents. This study is confined to even (A, Z) parent nuclei, referring to lead or neighboring nuclei as a daughter product, except for ^{230}Th in which the daughter is ^{206}Hg. Here, in PCM, the cluster is assumed to be preformed in the decaying nucleus with a specific probability of preformation, thereby providing us the structural information regarding the decaying fragments. Note that in above published works, a phenomenological approach

*rajni.mittal1989@gmail.com

(Blocki based nuclear potential [22]) was used; however, in the present study, a semi-microscopic method such as the Skyrme energy density formalism (SEDF) [23–29] is adopted. It is of interest to investigate the influence of Skyrme forces on the potential energy surfaces (PES) of these nuclei. The comparative analysis of SIII [30], SAMi [31], and SkI4 [32] forces is worked out in context of the most probable cluster configuration emitted across ^{208}Pb daughter nuclei. The choice of considered forces is based on the fact that all Skyrme forces have different contributions to the spin-orbit strength. In the standard Skyrme functional (SIII) spin-orbit potential is proportional to the single parameter of spin-orbit strength, i.e., W_0, or we can say that in the SIII force $W_0 = W_0'$. However in SkI4 and SAMi forces, double spin-orbit parameters are included such that $W_0 \neq W_0'$ [31,32].

Various structural aspects have been investigated in terms of behavioral patterns of fragmentation potential, shell effects, barrier modification (in terms of height and width), and fine structure (or substructure) of decaying fragments. The possible role of spin orbit potential has been worked out in terms of fragmentation potential and hence the preformation probability. We have performed our calculations by considering the Coulomb and nuclear interaction potentials as an interacting barrier for spherical consideration of the fragments. The half-lives in PCM are the result of the combined effects of preformation P_0 and penetration P probabilities, and are highly sensitive to the potential barrier. The estimated $T_{1/2}$ values have been compared with the available experimental data [33,34] to emphasize the relevance and applicability of the formalism used. In the present work, in addition to cluster radioactivity, the α-decay process of considered parents is also investigated using the same model. The calculated logarithmic half-lives of all α emitters is compared with the experimental data [35].

The paper is organized as follows: the methodology, which includes preformed cluster model (PCM) and the Skyrme energy density formalism, is presented in Sec. II. Calculations and results are discussed in Sec. III, and finally the outcomes are summarized in Sec. IV.

II. METHODOLOGY

A. The preformed cluster model (PCM)

The quantum mechanical fragmentation theory (QMFT) [36,37] is used to develop the preformed cluster model (PCM) [14–18]. The PCM is worked out in terms of the collective coordinates of mass and charge asymmetries $\eta = \frac{A_1-A_2}{A_1+A_2}$ and $\eta_Z = \frac{Z_1-Z_2}{Z_1+Z_2}$, the relative separation R, and the multipole deformations $\beta_{\lambda i}$ and orientations θ_i ($i = 1, 2$) of daughter and cluster nuclei.

Within PCM, the decay half-life $T_{1/2}$ is calculated by using the well known relation

$$\lambda = \frac{\ln 2}{T_{1/2}} = P_0 \nu_0 P. \tag{1}$$

Here λ and ν_0 respectively are the decay constant and barrier assault frequency. P_0 is the cluster (and daughter) preformation probability and P the barrier penetrability, which refer, respectively, to the η and R motions.

In the above equation, P_0 is obtained by solving the stationary Schrödinger equation in the η coordinate, at a fixed $R = R_a$,

$$\left[-\frac{\hbar^2}{2\sqrt{B_{\eta\eta}}}\frac{\partial}{\partial\eta}\frac{1}{\sqrt{B_{\eta\eta}}}\frac{\partial}{\partial\eta} + V_R(\eta)\right]\psi^{\omega}(\eta) = E^{\omega}\psi^{\omega}(\eta), \tag{2}$$

which on proper normalization gives

$$P_0 = \sqrt{B_{\eta\eta}}|\psi[\eta(A_i)]|^2(2/A), \tag{3}$$

with $i = 1$ or 2 and $\omega = 0, 1, 2, 3, \ldots$. For ground state decay, Eq. (2) is solved for $\omega = 0$ only.

The penetrability P in Eq. (2) is calculated by solving the WKB integral between R_a and R_b, the first and second turning points, respectively (see Fig. 1). In the WKB approximation, the transmission probability P is divided into three processes: (a) the penetrability P_i from R_a to R_i, (b) the (inner) deexcitation probability W_i at R_i, taken as unity, i.e., $W_i = 1$ for heavy cluster-decays [38], and (c) the penetrability P_b from R_i to R_b, giving

$$P = P_i W_i P_b, \tag{4}$$

where P_i and P_b are definedas

$$P_i = \exp\left[-\frac{2}{\hbar}\int_{R_a}^{R_i}\{2\mu[V(R) - V(R_i)]\}^{1/2}dR\right], \tag{5}$$

$$P_b = \exp\left[-\frac{2}{\hbar}\int_{R_i}^{R_b}\{2\mu[V(R) - Q]\}^{1/2}dR\right], \tag{6}$$

For R_a, the first turning point of the penetration path,

$$\begin{aligned} R_a(\eta) &= R_1 + R_2 + \Delta R \\ &= R_t(\eta) + \Delta R, \end{aligned} \tag{7}$$

where the η dependence of R_a is contained in R_t, and ΔR is a parameter assimilating the neck formation effects, somewhat similar to that used in the two-center shell model.

The structure information of the decaying nucleus is contained in P_0 via the fragmentation potential $V_R(\eta)$ and is defined as

$$\begin{aligned} V_R(\eta) = &-\sum_{i=1}^{2}[B_i(A_i, Z_i)] + V_C(R, Z_i) \\ &+V_N(R, A_i) + V_\ell(R, A_i). \end{aligned} \tag{8}$$

V_C, V_N, and V_ℓ are, respectively, the Coulomb, nuclear, and angular momentum dependent potentials for deformed and oriented nuclei (for details, refer to Refs. [39,40]). Note that shell effects enter here mainly through the ground state binding energies $B_i(A_i, Z_i)$ [41,42]. For ground state decays, $\ell = 0$ is a good approximation [34].

In Eq. (8), the nuclear potential V_N is calculated within the framework of the Skyrme energy density formalism (SEDF), which is described in the next section.

B. Skyrme energy density formalism (SEDF)

In the Skyrme energy density formalism (SEDF) [23,43], the nuclear interaction potential $V_N(R)$ between two colliding

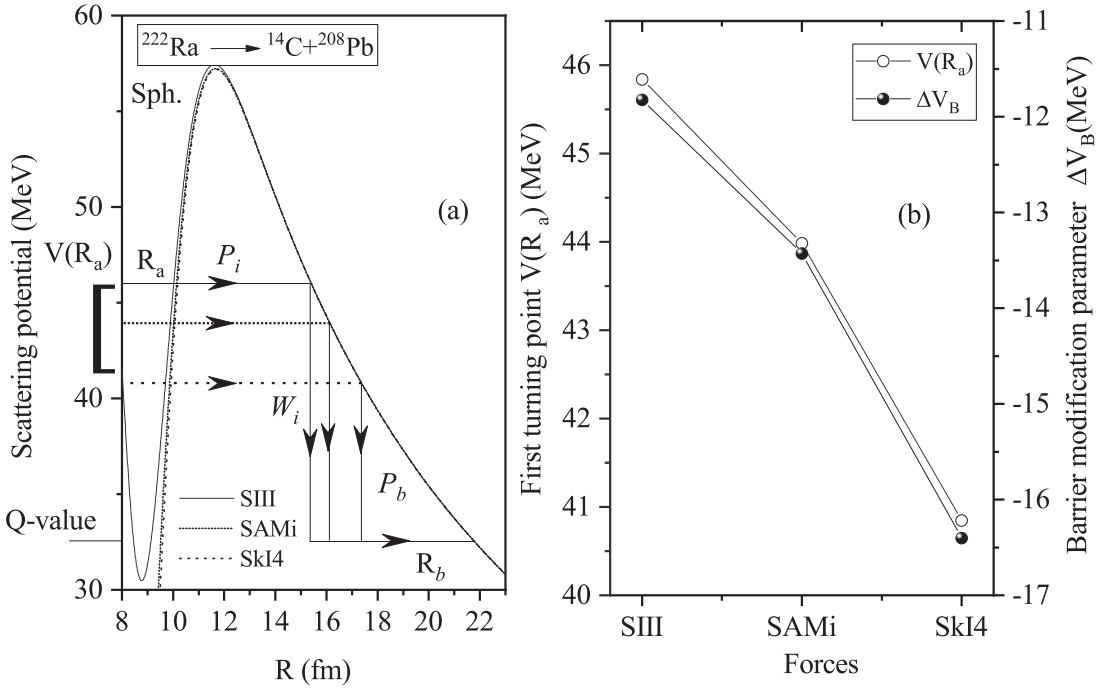

FIG. 1. (a) Variation of scattering potential with SIII, SkI4, and SAMi Skyrme forces for the decay of ^{222}Ra into spherical ^{14}C cluster and ^{208}Pb daughter. (b) Two-panel figure with the left side representing the value of the potential at first tunneling point $V(R_a)$ with the right side showing the barrier lowering parameter ΔV_B.

nuclei is defined as

$$V_N(R) = E_{\rm tot}(R) - E_1 - E_2, \tag{9}$$

where $E_{\rm tot}(R)$ is the total energy expectation value of the colliding parters at distance R (center to center), whereas the individual energies of non-interacting projectile and target nuclei are represented by E_1 and E_2. The energy expectation values $E_{\rm tot}(R)$, E_1 and E_2, are further obtained by volume integration of Hamiltonian density $H(r)$ as

$$E_{\rm tot}(R) = \int H[\rho_p(\vec{r}), \rho_n(\vec{r})]d\vec{r}, \tag{10}$$

$$E_i(R) = \int H[\rho_{ip}(\vec{r}), \rho_{\rm in}(\vec{r})]d\vec{r} \quad (i = 1, 2). \tag{11}$$

Here $\rho_{ip}(r)$, $\rho_{\rm in}(r)$ are proton and neutron densities of non-interacting nuclei, and $\rho_p(r)$, $\rho_n(r)$ are densities of interacting nuclei. $H(r)$ in the above equation stands for the energy density functional, given as in [23], including the kinetic energy contribution $\tau(r)$ and nuclear interaction parts $H_{\rm sky}(r)$:

$$H(\rho, \tau, \vec{J}) = \frac{\hbar^2}{2m}\tau + H_{\rm sky}(r). \tag{12}$$

The kinetic energy density τ is then calculated by using the extended Thomas fermi approximation of Bartel *et al.* [28].

The Skyrme Hamiltonian is given by [23]

$$\begin{aligned}
H_{\rm sky}(r) =& \tfrac{1}{2}t_0\big[\big(1+\tfrac{1}{2}x_0\big)\rho^2 - \big(x_0+\tfrac{1}{2}\big)\big(\rho_n^2+\rho_p^2\big)\big] \\
&+ \tfrac{1}{12}t_3\rho^\alpha\big[\big(1+\tfrac{1}{2}x_3\big)\rho^2 - \big(x_3+\tfrac{1}{2}\big)\big(\rho_n^2+\rho_p^2\big)\big] \\
&+ \tfrac{1}{4}\big[t_1\big(1+\tfrac{1}{2}x_1\big) + t_2\big(1+\tfrac{1}{2}x_2\big)\big]\rho\tau \\
&- \tfrac{1}{4}\big[t_1\big(x_1+\tfrac{1}{2}\big) - t_2\big(x_2+\tfrac{1}{2}\big)\big](\rho_n\tau_n + \rho_p\tau_p) \\
&+ \tfrac{1}{16}\big[3t_1\big(1+\tfrac{1}{2}x_1\big) - t_2\big(1+\tfrac{1}{2}x_2\big)\big](\vec{\nabla}\rho)^2 \\
&- \tfrac{1}{16}\big[3t_1\big(x_1+\tfrac{1}{2}\big) + t_2\big(x_2+\tfrac{1}{2}\big)\big] \\
&\times [(\vec{\nabla}\rho_n)^2 + (\vec{\nabla}\rho_p)^2] \\
&+ \tfrac{1}{2}W_0[\rho\vec{\nabla}\cdot\vec{J}] + \tfrac{1}{2}W_0'[\rho_n\vec{\nabla}\cdot\vec{J}_n + \rho_p\vec{\nabla}\cdot\vec{J}_p] \\
&- \big[\tfrac{1}{16}(t_1x_1 + t_2x_2)\vec{J}^2 - \tfrac{1}{16}(t_1 - t_2)\big(\vec{J}_p^2 + \vec{J}_n^2\big)\big].
\end{aligned} \tag{13}$$

The nuclear, kinetic energy, and spin-orbit densities are represented by $\rho = \rho_n + \rho_p$, $\tau = \tau_n + \tau_p$, and $\vec{J} = \vec{J}_n + \vec{J}_p$. m is the nucleon mass, and x_j, t_j $(j = 0, 1, 2)$, x_3, t_3, α, W_0, and W_0' refer to the Skyrme force parameters. In Eq. (13), the last two terms of the Hamiltonian correspond to the spin-orbit effect. In this work, we have used SIII, SkI4 [32], and SAMi [31] Skyrme forces.

In the above equation, spin density $\vec{J}$ is given by

$$\vec{J}_q(\vec{r}) = -\frac{2m}{\hbar^2}\frac{1}{2}W_0\frac{1}{f_q}\rho_q\vec{\nabla}(\rho + \rho_q). \tag{14}$$

Note that each of τ_q, f_q, and $\vec{J}_q$ are functions of ρ_q and/or ρ alone.

Densities of the composite system $\rho = \rho_1 + \rho_2$, with $\rho_i = \rho_{\rm in} + \rho_{ip}$ $(i = 1, 2)$, and $\tau(\rho)$ and $\vec{J}(\rho)$ are added under the frozen density approximation, as follows:

$$\begin{aligned}
\tau(\rho) &= \tau_1(\rho_1) + \tau_2(\rho_2), \\
\vec{J}(\rho) &= \vec{J}_1(\rho_1) + \vec{J}_2(\rho_2),
\end{aligned} \tag{15}$$

with $\rho_i = \rho_{\rm in} + \rho_{ip}$, $\tau_i(\rho_i) = \tau_{\rm in}(\rho_{\rm in}) + \tau_{ip}(\rho_{ip})$, and $\vec{J}_i(\rho_i) = \vec{J}_{\rm in}(\rho_{\rm in}) + \vec{J}_{ip}(\rho_{ip})$.

For the proximity potential, Gupta *et al.* [44] introduced the slab approximation of semi-infinite nuclear matter with surfaces parallel to the xy plane, moving in the z direction, and separated by distance s having minimum value s_0. Then, the interaction potential $V_N(R)$ between two nuclei separated by $R = R_1 + R_2 + s$ is given as

$$\begin{aligned} V_N(R) &= 2\pi\bar{R}\int_{s_0}^{\infty} e(s)ds = 2\pi\bar{R}\int\{H(\rho,\tau,\vec{J}) \\ &\quad - [H_1(\rho_1,\tau_1,\vec{J}_1) + H_2(\rho_2,\tau_2,\vec{J}_2)]\}dz \\ &= 2\pi\bar{R}\int\{(H(\rho) - [H_1(\rho_1) + H_2(\rho_2)]) \\ &\quad + (H(\vec{J}) - [H_1(\vec{J}_1) + H_2(\vec{J}_2)])\}dz \\ &= V_P(R) + V_J(R). \end{aligned} \tag{16}$$

Here, $V_P(R)$ and $V_J(R)$ are spin-orbit density independent and dependent parts of the nuclear interaction potential. $\bar{R}$ is the mean curvature radius defining the geometry of the system. Hence the nuclear potential derived within the SEDF approach is a sum of spin-orbit dependent (V_J) and independent (V_P) parts.

III. RESULTS AND DISCUSSION

A. Cluster radioactivity using Skyrme forces

In order to look for the extensive role of Skyrme forces, the barrier profile is analyzed for the spherical choice of cluster and daughter. Figure 1(a) shows the comparison of scattering potential (MeV) with the different Skyrme forces (SIII, SkI4, and SAMi) for the decay of ^{222}Ra into the most probable channel $^{14}\mathrm{C} + ^{208}\mathrm{Pb}$. It is evident from the figure that all considered Skyrme forces have similar barrier height, but other characteristics of the barrier such as the oscillator frequency ($\hbar\omega$) and potential at first turning point [$V(R_a)$] change considerably. Moreover, within PCM, fragments follow the two-step penetration process (explained in Sec. II), i.e., path 1 from R_a to R_i and path 2 from R_i to R_b [marked in Fig. 1(a)]. It is observed that the values of potentials at above mentioned points are different for considered Skyrme forces as penetration starts at a lower value of $V(R_a)$ for the SkI4 force and at higher magnitude for the SIII force. It also means that different Skyrme forces provide different penetration path and consequently impart corresponding modifications in penetration probability (P) of the cluster/daughter. The potential at the first turning point and at the top of the barrier V_B is then used to calculate the barrier lowering parameter ΔV_B, i.e.,

$$\Delta V_B = V(R_a) - V_B. \tag{17}$$

The effective "barrier lowering" parameter ΔV_B is an inbuilt property of the PCM and is estimated in reference to the unique choice of ΔR for a best fit to the data (discussed later). Note, since ΔV_B is defined as a negative quantity, the actually used barrier is effectively lowered. The left side of Fig. 1(b) shows the calculated values of $V(R_a)$, and on the right side scale ΔV_B is depicted. The result shows that different Skyrme forces require different modification in the barrier as the SIII force has a higher value of ΔV_B than the other two forces chosen. This discussion implies that choice of force plays an important role in deciding the penetration path.

Further, to identify the most probable cluster and daughter in the exit channel, SIII, SAMi, and SkI4 Skyrme forces are applied to examine the fragmentation structure of ^{222}Ra, ^{226}Ra, ^{232}U, and ^{234}U parent nuclei. Figure 2 depicts the variation of fragmentation potential V (MeV) as a function of fragment mass A_2 plotted at fitted values of neck length ΔR. It is clear from Figs. 2(a)–2(d) that, although there is a difference in the magnitudes of fragmentation potential, the potential energy structures (PES) remain similar for all considered Skyrme forces. For ^{222}Ra and ^{226}Ra parent nuclei, minimum potential is obtained with the SkI4 force and maximum with the SIII force. However, for the isotopes of U nucleus, a mixed trend is observed. In addition to this, despite the use of different Skyrme forces, the most favorable clusters (indicated with the solid vertical line) emitted from the respective parent nuclei remain intact, as the strongest minima in the fragmentation plot of ^{222}Ra, ^{226}Ra, ^{232}U, and ^{234}U parents correspond to ^{14}C, ^{14}C, ^{24}Ne, and ^{26}Ne clusters respectively (marked in Fig. 2). In the previous analysis using PCM [45], a similar result was obtained with the use of different proximity potentials. Importantly, the choice of the most probable cluster for all parents signifies the role of the shell closure effect, as the daughter nucleus that corresponds to these parent nuclei belongs to doubly magic ^{208}Pb or a neighboring isotope. Moreover, other clusters having a potential nearer to that of the experimentally verified clusters in the decay of the same parent nucleus are ruled out, either because of their smaller penetrability P or large calculated decay half-lives.

The computed Q value, which represents the available energy for clusters to penetrate the potential barrier, is shown in Fig. 3. The maximum in the Q value increases the penetration probability, which enhances the probable existence of a particular decay mode. Interestingly the ^{222}Ra nucleus is found to be unstable ($Q > 0$) against several cluster decays. The systematics of the Q value prefers the emission of heavier clusters (^{10}B, ^{14}C, ^{20}O, etc.) in the decay of the ^{222}Ra parent nucleus.

The above findings are better understood in terms of preformation probability and penetrability calculated in reference to the most favorable cluster in the decay of ^{222}Ra to ^{238}Pu parent nuclei by employing a spherical approach with the considered Skyrme forces. The results are respectively given in Tables I and II. The experimentally observed clusters and daughters of respective parents are also mentioned in the tables. It is evident from the Table I that, with the increase in mass number of the parent nuclei, the most probable clusters shift toward heavier mass. Table II depicts the the comparison of PCM calculated half-life with experimentally available data. It is to be noted here the the assault frequency ν_0 is constant ($=10^{21}$ s^{-1}) for all cluster decays. To address the half-lives, a fitting parameter, neck length ΔR, of the order of 0.85 ± 0.5 fm is used. It is evident from the Table II that PCM calculated half-lives with the choice of all three Skyrme forces (SIII, SAMi, SkI4) give reasonable agreement with experimentally observed data for all nuclei ranging from ^{222}Ra

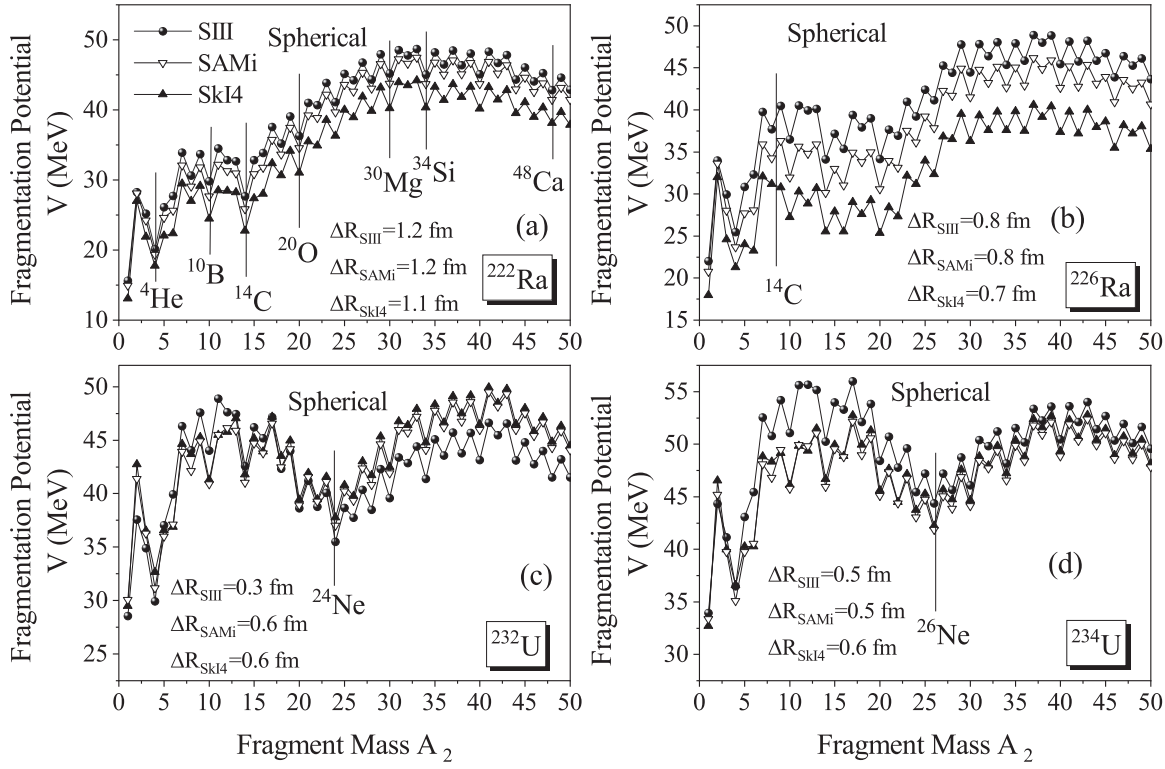

FIG. 2. Fragmentation potentials of (a) ^{222}Ra (b) ^{226}Ra (c) ^{232}U, and (d) ^{234}U parent nuclei for spherical choice of decaying fragments using SIII, SAMi, and SkI4 Skyrme forces. The figure is plotted at fitted values of neck-length parameter ΔR.

to ^{230}U. Specifically for ^{232,234}U, ^{236}Pu, and ^{238}Pu nuclei, the deviation of PCM predicted half lives with respect to experimental data is fairly small for the SIII force as compared to other forces. Conclusively, the choice of Skyrme force has a crucial influence in determining the tunnelling path and hence half-life of respective clusters. Figure 4 shows the P_0 and P of the ^{222}Ra, ^{228}Th, ^{230}U, and ^{236}Pu parent nuclei decaying into the ^{208}Pb daughter nucleus plotted with the SIII force only. After obtaining the P_0 and P values of all preferred clusters, their decay half-lives are calculated in reference to Eq. (1). Within PCM, logarithmic half-life times [$\log_{10} T_{1/2}$ (s)] are the combined effect of cluster preformation probability and its penetration probability across the barrier, and are depicted in the lower panel of Fig. 4.

Moreover, to see the relevance of the considered Skyrme forces used in the context of cluster radioactivity, the standard

TABLE I. PCM calculated preformation probability P_0 and penetrability P for the most probable clusters emitted from different parents using SIII, SAMi, and SkI4 forces.

	SIII		SAMi		SkI4	
Parent	P_0	P	P_0	P	P_0	P
^{222}Ra $\rightarrow$ ^{14}C + ^{208}Pb	1.74×10^{-16}	2.06×10^{-19}	2.42×10^{-18}	2.04×10^{-19}	9.80×10^{-14}	3.93×10^{-15}
^{224}Ra $\rightarrow$ ^{14}C + ^{210}Pb	5.89×10^{-16}	8.69×10^{-23}	8.17×10^{-15}	7.95×10^{-25}	1.08×10^{-11}	6.75×10^{-14}
^{226}Ra $\rightarrow$ ^{14}C + ^{212}Pb	2.74×10^{-18}	3.05×10^{-26}	2.18×10^{-17}	1.19×10^{-27}	1.60×10^{-12}	5.52×10^{-32}
^{226}Th $\rightarrow$ ^{18}O + ^{208}Pb	8.23×10^{-22}	1.68×10^{-19}	4.51×10^{-21}	8.64×10^{-20}	8.38×10^{-19}	2.57×10^{-19}
^{226}Th $\rightarrow$ ^{14}C + ^{212}Po	1.21×10^{-20}	3.68×10^{-22}	1.82×10^{-20}	1.37×10^{-18}	3.08×10^{-15}	5.37×10^{-26}
^{228}Th $\rightarrow$ ^{20}O + ^{208}Pb	6.25×10^{-18}	1.48×10^{-25}	5.15×10^{-16}	1.65×10^{-24}	1.68×10^{-11}	1.84×10^{-29}
^{230}Th $\rightarrow$ ^{24}Ne + ^{206}Hg	2.84×10^{-19}	3.76×10^{-29}	9.45×10^{-19}	1.58×10^{-27}	2.07×10^{-13}	7.25×10^{-30}
^{230}U $\rightarrow$ ^{22}Ne + ^{208}Pb	1.64×10^{-21}	1.03×10^{-23}	6.84×10^{-13}	6.41×10^{-27}	3.75×10^{-17}	1.58×10^{-25}
^{232}U $\rightarrow$ ^{24}Ne + ^{208}Pb	1.07×10^{-16}	7.29×10^{-29}	3.43×10^{-15}	4.49×10^{-26}	7.13×10^{-12}	3.97×10^{-25}
^{234}U $\rightarrow$ ^{26}Ne + ^{208}Pb	2.73×10^{-20}	1.56×10^{-28}	1.98×10^{-14}	5.48×10^{-29}	1.62×10^{-13}	6.14×10^{-29}
^{236}Pu $\rightarrow$ ^{28}Mg + ^{208}Pb	7.34×10^{-17}	1.26×10^{-26}	1.17×10^{-19}	6.381×10^{-22}	6.77×10^{-15}	5.92×10^{-25}
^{238}Pu $\rightarrow$ ^{30}Mg + ^{208}Pb	2.60×10^{-18}	5.92×10^{-29}	1.19×10^{-18}	1.54×10^{-25}	3.31×10^{-13}	1.43×10^{-27}

TABLE II. Calculated half-life times and other characteristic quantities for cluster decay of various parent nuclei to the ground states of their respective daughter nuclei. Calculations are made by using the PCM for cases of SIII, SAMi, and SkI4 forces and compared with experimental data [33,34].

				Half-lives ($\log_{10} T_{1/2}$) (s)				
	ΔR (fm)			PCM				
Decay channel	SIII (a)	SAMi (b)	SkI4 (c)	SIII (a)	SAMi (b)	SkI4 (c)	Expt.	Q value (MeV)
$^{222}\text{Ra} \rightarrow {}^{14}\text{C} + {}^{208}\text{Pb}$	1.2	1.2	1.1	12.81	11.60	10.77	11.01	32.47
$^{224}\text{Ra} \rightarrow {}^{14}\text{C} + {}^{210}\text{Pb}$	0.8	0.8	0.9	15.66	16.50	12.51	15.86	31.16
$^{226}\text{Ra} \rightarrow {}^{14}\text{C} + {}^{212}\text{Pb}$	0.8	0.8	0.7	21.47	21.98	21.45	21.79	28.61
$^{226}\text{Th} \rightarrow {}^{18}\text{O} + {}^{208}\text{Pb}$	1.0	1.0	1.1	18.20	17.75	15.20	15.3	47.55
$^{226}\text{Th} \rightarrow {}^{14}\text{C} + {}^{212}\text{Po}$	1.0	1.4	0.8	19.7	15.94	18.15	15.3	31.70
$^{228}\text{Th} \rightarrow {}^{20}\text{O} + {}^{208}\text{Pb}$	0.6	0.8	0.1	20.4	17.4	17.88	20.87	45.91
$^{230}\text{Th} \rightarrow {}^{24}\text{Ne} + {}^{206}\text{Hg}$	0.35	0.6	0.6	25.30	23.18	20.18	24.61	58.57
$^{230}\text{U} \rightarrow {}^{22}\text{Ne} + {}^{208}\text{Pb}$	0.5	0.5	0.6	22.0	16.68	19.55	18.2	61.69
$^{232}\text{U} \rightarrow {}^{24}\text{Ne} + {}^{208}\text{Pb}$	0.3	0.6	0.6	22.43	18.16	13.89	21.05	62.03
$^{234}\text{U} \rightarrow {}^{26}\text{Ne} + {}^{208}\text{Pb}$	0.5	0.6	0.7	25.72	20.33	19.38	25.06	58.65
$^{236}\text{Pu} \rightarrow {}^{28}\text{Mg} + {}^{208}\text{Pb}$	0.3	0.7	0.6	20.33	18.46	16.73	21.67	78.75
$^{238}\text{Pu} \rightarrow {}^{30}\text{Mg} + {}^{208}\text{Pb}$	0.3	0.6	0.6	24.13	21.09	17.67	25.70	76.82

rms deviation (σ) with the half-lives of experimentally observed clusters is calculated for SIII, SAMi, and SkI4 Skyrme forces as shown in Fig. 5. The formula used for σ calculation is mentioned in the figure. It is observed that the standard rms deviation in half-lives with respect to the experimental $\log_{10} T_{1/2}$ is minimum with the SIII force and starts increasing for SAMi and SkI4 Skyrme forces. Thus one may conclude that the SIII force is perhaps the best option to study cluster radioactivity of the considered parent nuclei.

In addition, the role of spin-orbit potential is investigated in the cluster dynamics of the considered systems. Since the SIII force is able to provide cluster half-lives closer to experimental half-lives, the present study is conducted with the SIII force only. Figure 6 depicts the variation of preformation probability (P_0) of various fragments emitted from ^{222}Ra, ^{226}Ra, ^{226}Th, and ^{228}Th parents with and without considering the spin-orbit potential V_J in the total interaction potential. It is observed from the figure that the magnitude of P_0 of decaying fragments changes significantly when the contribution of spin-orbit potential V_J is switched off from the total interaction potential. The P_0 and P values of all experimentally observed clusters, with the exclusion of the spin-orbit part, are depicted in Table III. The role of spin-orbit effects is further investigated in

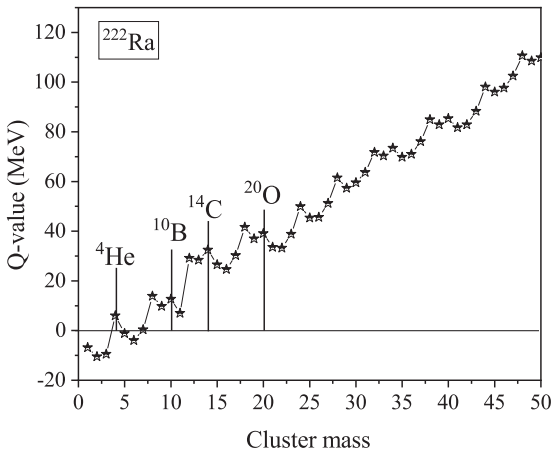

FIG. 3. Variation of Q value of clusters emitted from the ^{222}Ra parent nucleus.

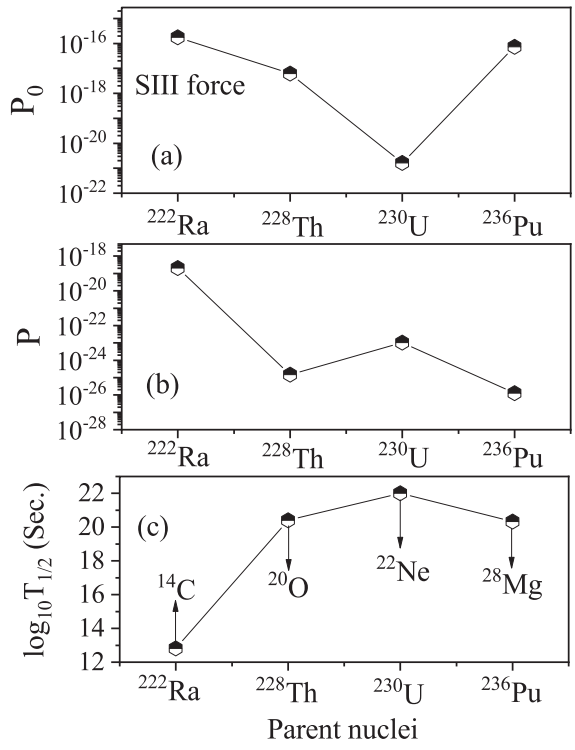

FIG. 4. Variation of P_0, P, and half-lives of clusters emitted from different parent nuclei calculated using the SIII force.

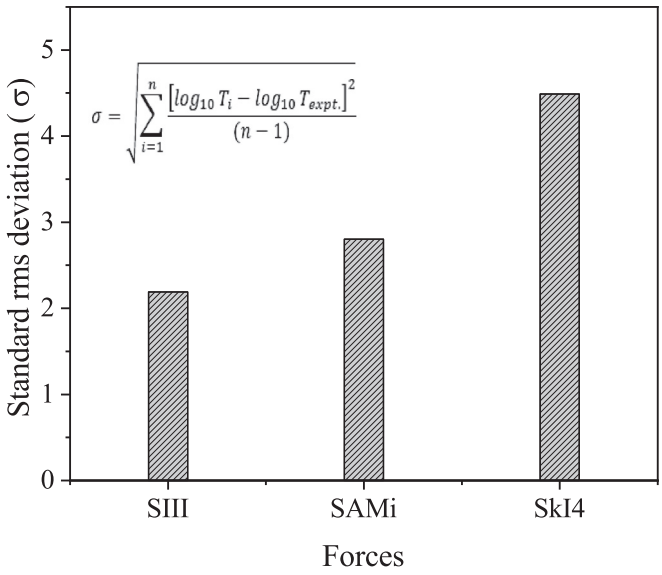

FIG. 5. Standard rms deviation (σ) calculated for SIII, SAMi, and SkI4 Skyrme forces.

Table IV by calculating the percentage change in the PCM calculated cluster half-lives with and without the inclusion of V_J, calculated as

$$\%\Delta \log t_{1/2} - I = \left| \frac{\log t_{1/2}(\text{with } V_J) - \log t_{1/2}(\text{without } V_J)}{\log t_{1/2}(\text{with } V_J)} \right| \times 100,$$

TABLE III. PCM calculated preformation probability P_0 and penetrability P without considering spin-orbit effects in SIII force.

Parent	P_0	P
^{222}Ra	0.136×10^{-15}	0.165×10^{-18}
^{224}Ra	0.133×10^{-12}	0.419×10^{-24}
^{226}Ra	0.264×10^{-19}	0.794×10^{-27}
^{226}Th	0.241×10^{-20}	0.450×10^{-19}
^{226}Th	0.864×10^{-23}	0.259×10^{-25}
^{230}U	0.402×10^{-15}	0.423×10^{-26}
^{234}U	0.892×10^{-12}	0.727×10^{-32}

and the last column represents the percentage change in the PCM calculated half-life $\log t_{1/2}$ (without including spin-orbit potential) vs experimentally given values, marked as $\%\Delta \log t_{1/2}$ II. It is found from the second column of Table IV that half-lives show a considerable difference of 37% when the spin-orbit potential is excluded from the nuclear interaction potential. This deviation becomes more remarkable when compared with the last column of Table IV. This suggest that the spin-orbit effects are significantly important in the cluster radioactivity process. It is important to mention here that in the table half-lives of clusters with parent nuclei are shown up to ^{234}U. The reason is that the half-lives of the remaining clusters cannot be calculated, as the potential at the first turning point turns out to be less than the Q value of the decay. To clarify this point, Fig. 7 is plotted without considering spin-orbit effects. In the figure the variation of $V(R_a) - Q_{\text{value}}$ on the y axis with mass of the parent nuclei

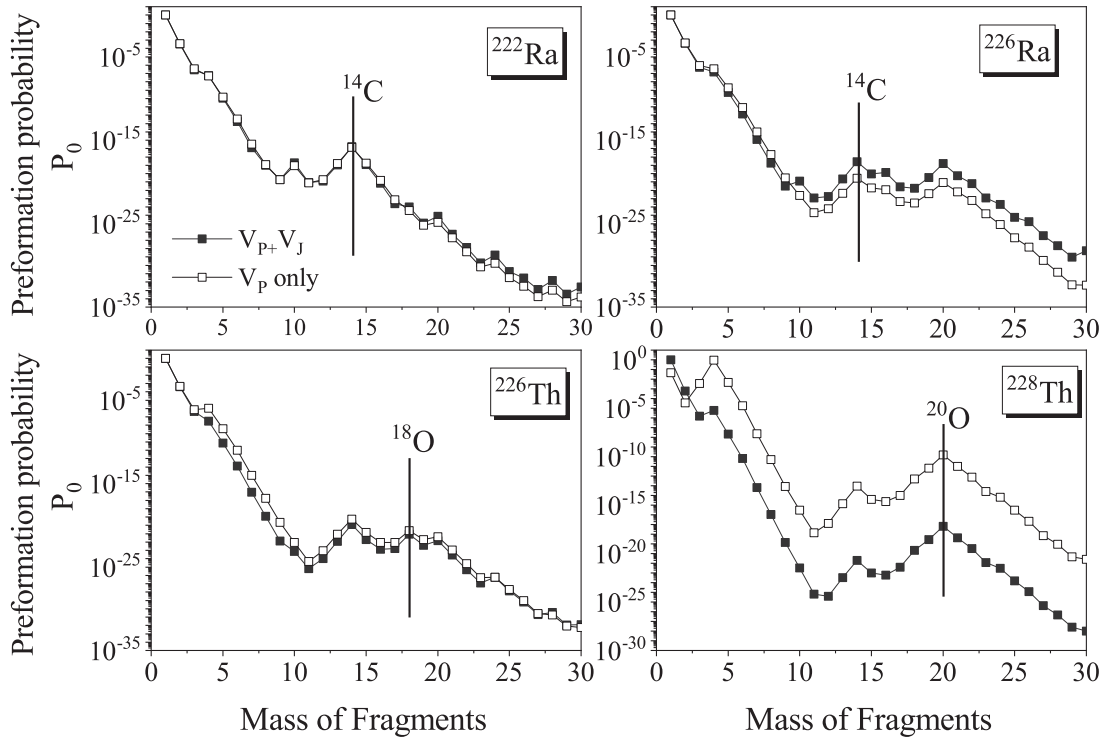

FIG. 6. Preformation probability P_0 of ^{222}Ra, ^{226}Ra, ^{226}Th, and ^{228}Th parent nuclei with and without considering the spin-orbit potential within the SIII force.

TABLE IV. Column 2 refers the percentage change in PCM calculated half-live ($\%\Delta \log t_{1/2}$ I) with and without considering spin-orbit effects, and column 3 depicts the percentage difference in PCM calculated $\log t_{1/2}$ (without including spin-orbit potential) vs experimentally given values ($\%\Delta \log t_{1/2}$ II).

Parent	$\%\Delta \log t_{1/2}$ I	$\%\Delta \log t_{1/2}$ II
^{222}Ra	1.5	18
^{224}Ra	0.1	1.4
^{226}Ra	16	18
^{226}Th	0.5	19
^{226}Th	37	76
^{230}U	8	10
^{234}U	12	10

(shown on the x axis) is depicted. It is evident from the figure that the difference $V(R_a) - Q_{\text{value}}$ is positive for ^{222}Ra to ^{234}U, which turns towards negative values for rest of the parent nuclei (for more details see Ref. [21]).

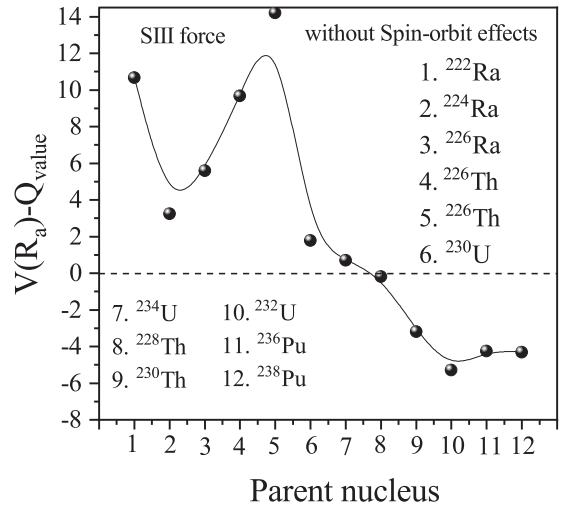

FIG. 7. Variation of $V(R_a) - Q_{\text{value}}$ as a function of mass of parent nuclei. The calculation is made without considering spin-orbit effects in the interaction potential.

B. α decay of even (A, Z) parent nuclei using the SIII force

Recently [46], Dumitrescu and Delion examined emission data for proton, α, and cluster radioactivity for a number of parent nuclei from ^{106}Te to ^{294}Og in a unified model by using a realistic analytical approach for the barrier penetration and spectroscopic factor. Following the above work, we have made an attempt to investigate α decay for the same parents (Ra, Th, U, and Pu) discussed in the previous section for the cluster decay. Within the framework of PCM, the logarithmic half-lives of all α emitters are calculated using the SIII force. The experimental data of α emission is taken from the table of [35]. The calculated results are presented in Table V. In the table, the preformation probability P_0 and penetrability P of the decay channel are shown along with the comparison of PCM calculated half-lives with experimentally available data. The Q values for α decay are also given in the table; they are calculated using the experimental and theoretical mass compilations of Audi-Wapstra and of Möller *et al.* [41,42]. It is observed from the table that the calculated logarithmic half-life values are in fair agreement with the available experimental data [35].

In our future work, we are interested to study the role of the above Skyrme forces in the ground state decay of superheavy elements (SHEs).

IV. SUMMARY

In this work, the cluster emission of various radioactive parent nuclei is investigated using the preformed cluster model (PCM). The study is carried out within the framework of the Skyrme energy density formalism (SEDF), and decay half-lives ($\log_{10} T_{1/2}$) of the clusters are estimated using different Skyrme forces (SIII, SkI4, and SAMi). It is observed that half-lives of the clusters change significantly with the use of different Skyrme forces, because of the corresponding change in the preformation probability (P_0) and penetration probability (P) of the emitted cluster. The chosen

TABLE V. The PCM calculated logarithmic half-lives of the α emitters along with daughters compared with the available experimental data [35]. The Q values, preformation probability P_0, and penetrability P of the decaying channel are also listed.

Parent	Daughter	P_0	P	$\log_{10} T_{1/2}^{\text{PCM}}$ (s)	$\log_{10} T_{1/2}^{\text{Expt.}}$ (s)	Q value (MeV)
^{222}Ra	^{218}Rn	5.29×10^{-8}	1.00×10^{-19}	4.7	1.6	5.996
^{224}Ra	^{220}Rn	3.85×10^{-6}	1.25×10^{-22}	5.7	5.5	5.886
^{226}Ra	^{222}Rn	1.51×10^{-7}	3.36×10^{-27}	11.8	10.7	4.886
^{226}Th	^{222}Ra	1.62×10^{-8}	2.05×10^{-18}	3.9	3.3	7.016
^{228}Th	^{224}Ra	8.87×10^{-8}	1.31×10^{-22}	7.4	7.8	5.526
^{230}Th	^{226}Ra	5.58×10^{-9}	8.91×10^{-27}	12.7	12.4	4.726
^{230}U	^{226}Th	1.40×10^{-7}	8.32×10^{-22}	7.3	6.3	5.646
^{232}U	^{228}Th	1.54×10^{-7}	1.53×10^{-25}	10.1	9.3	5.146
^{234}U	^{230}Th	2.32×10^{-8}	7.63×10^{-28}	13.2	12.9	4.706
^{236}Pu	^{232}U	1.49×10^{-7}	2.25×10^{-23}	7.9	8.0	5.776
^{238}Pu	^{234}U	1.54×10^{-8}	1.35×10^{-24}	10.1	9.4	5.586

Skyrme forces adequately address the half-lives of clusters emitted from parent nuclei with mass $A = 222$–234, and SIII seems to perform relatively better for heavier nuclei. Here, the effect of a spin-orbit density dependent potential on $\log_{10} T_{1/2}$ is examined in reference to the SIII force. Beside this, α decay is also examined using the same model, and half-lives are addressed within the limits of experimental data.

ACKNOWLEDGMENTS

One of us (R.) is thankful to the Council of Scientific and Industrial Research (CSIR), New Delhi [Files No. 09/0677(11733)/2021-EMR-I and No. 09/1007(13391)/2022-EMR-I) for providing financial support to carry out this work. M.K.S. is thankful to DST-SERB for Grant No. CRG/2021/001144.

[1] R. Bonetti and A. Guglielmetti, Rom. Rep. Phys. **59**, 301 (2007).
[2] R. Bonetti, C. Chiesa, A. Guglielmetti, C. Migliorino, A. Cesana, and M. Terrani, Nucl. Phys. A **556**, 115 (1993).
[3] A. A. Ogloblin, R. Bonetti, V. A. Denisov, A. Guglielmetti, M. G. Itkis, C. Mazzocchi, V. L. Mikheev, Yu. Ts. Oganessian, G. A. Pik-Pichak, G. Poli, S. M. Pirozhkov, V. M. Semochkin, V. A. Shigin, I. K. Shvetsov, and S. P. Tretyakova, Phys. Rev. C **61**, 034301 (2000).
[4] A. Sandulescu, D. N. Poenaru, and W. Greiner, Sov. J. Part. Nucl. **11**, 528 (1980).
[5] H. J. Rose and G. A. Jones, Nature (London) **307**, 245 (1984).
[6] D. N. Poenaru, R. A. Gherghescu, and W. Greiner, Phys. Rev. Lett. **107**, 062503 (2011); Phys. Rev. C **85**, 034615 (2012).
[7] D. D. Ni, Z. Z. Ren, T. K. Dong, and C. Xu, Phys. Rev. C **78**, 044310 (2008).
[8] D. N. Poenaru, R. A. Gherghescu, and W. Greiner, Phys. Rev. C **83**, 014601 (2011).
[9] M. Horoi, J. Phys. G: Nucl. Part. Phys. **30**, 945 (2004).
[10] C. Qi, F. R. Xu, R. J. liotta, and R. Wyss, Phys. Rev. Lett. **103**, 072501 (2009).
[11] G. Shanmugam and B. Kamalaharan, Phys. Rev. C **41**, 1742 (1990).
[12] G. Shanmugam, G. M. Carmel Vigila Bai, and B. Kamalaharan, Phys. Rev. C **51**, 2616 (1995).
[13] R. G. Lovas, R. J. Liotta, A. Insolia, K. Varga, and D. S. Delion, Phys. Rep. **294**, 265 (1998).
[14] S. K. Arun, R. K. Gupta, B. B. Singh, S. Kanwar, and M. K. Sharma, Phys. Rev. C **79**, 064616 (2009).
[15] S. K. Arun, R. K. Gupta, S. Kanwar, B. B. Singh, and M. K. Sharma, Phys. Rev. C **80**, 034317 (2009).
[16] G. Sawhney, M. K. Sharma, and R. K. Gupta, Phys. Rev. C **83**, 064610 (2011).
[17] G. Sawhney, K. Sandhu, M. K. Sharma, and R. K. Gupta, Eur. Phys. J. A **50**, 175 (2014).
[18] K. Sharma, G. Sawhney, M. K. Sharma, and R. K. Gupta, Eur. Phys. J. A. **55**, 30 (2019).
[19] X. J. Bao, H. F. Zhang, B. S. Hu, G. Royer, and J. Q. Li, J. Phys. G: Nucl. Part. Phys. **39**, 095103 (2012).
[20] G. Royer and R. Moustabchir, Nucl. Phys. A **683**, 182 (2001).
[21] R. Kumar and M. K. Sharma, Phys. Rev. C **85**, 054612 (2012).
[22] J. Błocki, J. Randrup, W. J. Swiatecki, and C. F. Tsang, Ann. Phys. (NY) **105**, 427 (1977).
[23] D. Vautherin and D. M. Brink, Phys. Rev. C **5**, 626 (1972).
[24] D. Vautherin, Phys. Rev. C **7**, 296 (1973).
[25] B. Grammoticos and A. Voros, Ann. Phys. **123**, 359 (1979).
[26] B. Grammoticos and A. Voros, Ann. Phys. **129**, 153 (1980).
[27] M. Brack, C. Guet, and H.-B. Hakansson, Phys. Rep. **123**, 275 (1985).
[28] J. Bartel and K. Bencheikh, Eur. Phys. J. A **14**, 179 (2002).
[29] R. K. Gupta, D. Singh, and W. Greiner, Phys. Rev. C **75**, 024603 (2007).
[30] J. Friedrich and P.-G. Reinhard, Phys. Rev. C **33**, 335 (1986).
[31] X. Roca-Maza, G. Colò, and H. Sagawa, Phys. Rev. C **86**, 031306(R) (2012).
[32] P.-G. Reinhard and H. Flocard, Nucl. Phys. A **584**, 467 (1995).
[33] R. Bonetti and A. Guglielmetti, in *Heavy Elements and Related New Phenomena*, edited by W. Greiner and R. K. Gupta (World Scientific, Singapore, 1999), Vol. II, p. 643.
[34] R. K. Gupta and W. Greiner, Int. J. Mod. Phys. E **03**, 335 (1994).
[35] D. S. Delion and A. Dumitrescu, At. Data Nucl. Data Tables **101**, 1 (2015) and references contained therein.
[36] J. Maruhn and W. Greiner, Phys. Rev. Lett. **32**, 548 (1974).
[37] R. K. Gupta, W. Scheid, and W. Greiner, Phys. Rev. Lett. **35**, 353 (1975).
[38] M. Greiner and W. Scheid, J. Phys. G: Nucl. Phys. **12**, L229 (1986).
[39] R. K. Gupta, S. K. Arun, R. Kumar, and Niyti, Int. Rev. Phys. **2**, 369 (2008).
[40] B. B. Singh, M. K. Sharma, and R. K. Gupta, Phys. Rev. C **77**, 054613 (2008).
[41] P. Möller, J. R. Nix, W. D. Myers, and W. J. Swiatecki, At. Data Nucl. Data Tables **59**, 185 (1995).
[42] G. Audi, A. H. Wapstra, and C. Thibault, Nucl. Phys. A **729**, 337 (2003).
[43] Rajni, D. jain, I. Sharma, and M. K. Sharma, Eur. Phys. J. A **53**, 208 (2017).
[44] P. Chattopadhyay and R. K. Gupta, Phys. Rev. C **30**, 1191 (1984).
[45] R. Kumar, Phys. Rev. C **86**, 044612 (2012).
[46] A. Dumitrescu and D. S. Delion, At. Data Nucl. Data Tables **145**, 101501 (2022).